ELSEVIER

ISPRS Journal of Photogrammetry & Remote Sensing 56 (2002) 177–194

PHOTOGRAMMETRY & REMOTE SENSING

www.elsevier.com/locate/isprsjprs

Processing of *Ikonos* imagery for submetre 3D positioning and building extraction

C.S. Fraser [a,*], E. Baltsavias [b], A. Gruen [b]

[a] *Department of Geomatics, University of Melbourne, Melbourne, 3010 Victoria, Australia*
[b] *Institute of Geodesy and Photogrammetry, ETH-Hoenggerberg, CH-8093 Zurich, Switzerland*

Received 22 June 2001; accepted 12 February 2002

Abstract

An investigation of the application of 1-m *Ikonos* satellite imagery to 3D point positioning and building reconstruction is reported. The focus of the evaluation of *Geo* panchromatic imagery has been upon 3D positioning accuracy, radiometric quality and attributes of the image data for building feature extraction. Following an initial review of characteristics of the *Ikonos* system, the multi-image dataset employed is described, as is the Melbourne *Ikonos* testfield. Radiometric quality and image preprocessing aspects are discussed, with attention being given to noise level and artifacts, as well as to methods of image enhancement. The results of 2D and 3D metric accuracy tests using straightforward geometric sensor models are summarised, these showing that planimetric accuracy of 0.3–0.6 m and height accuracy of 0.5–0.9 m are readily achievable with only three to six ground control points. A quantitative and qualitative assessment of the use of stereo *Ikonos* imagery for generating building models is then provided, using the campus of the University of Melbourne as an evaluation site. The results of this assessment are discussed, these highlighting the high accuracy potential of *Ikonos Geo* imagery and limitations to be considered in building reconstruction when a comprehensive and detailed modelling is required.

Keywords: *Ikonos*; Radiometric analysis; Sensor models; 3D point positioning; Building extraction

1. Introduction

Although it has now been 2 years since *Ikonos* imagery first became commercially available from Space Imaging, there have been relatively few accounts presented of photogrammetric analysis of this new image data. A number of factors have contributed to the current paucity of research outcomes related to the geometric and radiometric quality of 1-m panchromatic, 4-m multispectral and 1-m pan-sharpened *Ikonos* imagery. These include significant early delays in image delivery, restrictions regarding both the provision of stereo imagery and disclosure of the camera model and orbit ephemeris data, limited data availability and delays due to ongoing improvements within the image preprocessing phase. Also, it seems fair to say that teething problems were encountered with what is a commercially new technology being made available to the user community under a distinctly new business model (e.g. Gruen, 2000).

Published reports to date on photogrammetric aspects of *Ikonos* imagery have focussed mainly on the accuracy attainable in ortho-image generation (e.g. Davis and Wang, 2001; Kersten et al., 2000; Toutin and

* Corresponding author. Tel.: +61-3-8344-4117; fax: +61-3-9347-2916.
E-mail address: c.fraser@unimelb.edu.au (C.S. Fraser).

0924-2716/02/$ - see front matter
PII: S0924-2716(02)00045-X

Cheng, 2000; Toutin, 2001; Baltsavias et al., 2001; Jacobsen, 2001) and to a lesser degree on DTM extraction (Toutin et al., 2001; Muller et al., 2001), rather than upon accuracy aspects of feature extraction. Results concerning 3D positioning from stereo spatial intersection utilising a rigorous sensor orientation model are both few and mainly from Space Imaging (Dial, 2000; Grodecki and Dial, 2001), the results reported being more accurate than *Ikonos* product specifications would suggest. Investigations into 3D positioning using alternative models have recently been reported by Toutin et al. (2001) and Hu and Tao (2001).

As an initial investigative phase into the application of high-resolution spaceborne imagery for object feature point detection, recognition and reconstruction, early research had been performed using simulated data with empirical analysis. Ridley et al. (1997) evaluated the potential of 1-m resolution satellite imagery for building extraction, and findings were that only 73% and 86% of buildings could be interpreted correctly using monoscopic and stereoscopic imagery, respectively. More recently, Sohn and Dowman (2001) reported an investigation into building extraction from high-resolution imagery. However, the study dealt with large detached buildings only and a comprehensive analysis of accuracy and completeness in the modelling of structure detail was not performed. In a broader feature extraction context, Hofmann (2001) has reported on 2D detection of buildings and roads in *Ikonos* imagery using spectral information, a DSM derived from laser scanning, and image context and form via the commercial image processing package eCognition. Dial et al. (2001) have presented the results of investigations into automated road extraction, with the focus being upon wide suburban roads in expanding US cities, while experiences with semiautomated methods are reported in Gruen (2000).

A feature common to almost all published work to date on geometric processing of *Ikonos* imagery has been the use of ground control of insufficient accuracy to exploit the full metric potential of *Ikonos Geo* imagery. Given the present shortage of information on the performance of the *Ikonos* system for high-accuracy 3D positioning and feature extraction, it has been necessary in the reported investigation to examine essentially three salient aspects when evaluating the use of 1-m stereo imagery for 3D point positioning and building extraction in support of 3D city modelling. These comprise the geometric accuracy of 3D positioning from stereo and multi-image coverage; the radiometric quality, with an emphasis on characteristics to support automatic feature extraction (e.g. noise content, edge quality and contrast); and attributes of the imagery for the special application of building extraction and visual reconstruction. Here, we examine these aspects with the aid of threefold *Ikonos* coverage of a precisely surveyed testfield covering the city of Melbourne. We first describe this testfield dataset and then examine radiometric and image preprocessing aspects. This is followed by an evaluation of the metric potential of *Ikonos* mono, stereo and three-image coverage, along with an account of experimental application of stereo imagery to building reconstruction, including topology building and visualisation.

The basic sensor and mission parameters for the *Ikonos-2* satellite are provided at Space Imaging's web site (www.spaceimaging.com) and visitors to the site will note that there are basically five product options for panchromatic, multispectral and pan-sharpened 1-m *Ikonos* imagery: *Geo*, *Reference*, *Pro*, *Precision* and *Precision Plus*. Except for the *Geo* product, all are ortho-rectified using a DTM, with ground control being required for *Precision* and *Precision Plus* ortho-imagery. The absolute planimetric positioning accuracies (RMS, 1σ) associated with these categories of imagery are 24, 12, 5, 2 and 1 m, respectively. The error budget for *Geo* imagery does not include influences due to terrain relief, or possible additional errors due to projection of the imagery onto an "inflated" ellipsoid at a selected elevation (this elevation value was not provided in the metadata file until mid-2001). Depending on the intended function of a digital city model, metric accuracy expectations will vary, though if the very sizeable market of modelling for mobile communications is to be accommodated, accuracies at the metre level are generally sought. The clear implication from the product range listed above, however, is that users of *Ikonos* imagery who seek metre-level accuracy will have to resort to acquisition of *Precision* and *Precision Plus* imagery, which is 5–10 times more expensive than *Geo*. We have pursued an alternative option, with the aim of yielding high accuracy results, to metre or submetre level, using the least expensive *Ikonos* data, namely *Geo* images, coupled with alternative computational schemes for mono, stereo and multi-image point positioning.

2. Input data

2.1. Image data

The imagery comprised a stereopair of epipolar-resampled *Geo* panchromatic images and a nadir-looking scene of panchromatic and multispectral imagery. The latter were also combined to form a pan-sharpened image. As indicated in Table 1, the sensor and sun elevation angles for the stereopair, imaged in winter, were less than optimal. Apart from the right stereo image, the azimuths of sensor and sun differed considerably, leading to strong shadows in nonoccluded areas. The overall geometry was close to that of three-line imagery, with the base/height ratio of the stereopair being $B/H = 1.2$. Supplied with the stereo imagery were coefficients of the rational functions that provide a mechanism for object-to-image space transformation and 3D point positioning. There were initially no rational function coefficients (also termed RPCs) for the near-nadir image, since the option of obtaining these for mono *Geo* imagery was not available at the time the data was acquired. Although these were subsequently obtained, the present discussion of RPC-based 3D spatial intersection is restricted to the stereopair of *Geo* images. Features of three-image RPC spatial intersection are discussed in Fraser et al. (2002).

2.2. Melbourne Ikonos testfield

Covering an area of 7×7 km over central Melbourne, with an elevation range of less than 100 m, the testfield configuration considered comprises an array of 32 GPS-surveyed ground control points (GCPs), all being road roundabouts. The locations of the GCPs are shown in Fig. 1. As mentioned, feature extraction accuracies to metre level were sought from the stereo *Ikonos* data and, thus, there was a need to measure image-identifiable ground points to subpixel accuracy within the imagery, as well as to submetre precision on the ground. Road roundabouts were selected as control points since they constituted an elliptical target which was usually well contrasted against its background (the surrounding road) within the image, and which was typically 8–25 pixels in diameter. Within the imagery, it was the centroid of the roundabout that was measured and so the GPS survey needed also to determine the centre point coordinates. As described in Hanley and Fraser (2001), the centroids of each of the roundabouts were determined by measuring six or more edge points around the circumference of the feature, both in the image and on the ground, and then employing a best-fitting ellipse computed by least-squares to determine the ellipse centres. It was possible through this means to achieve accuracies of image and object point determination, in 2D and 3D space, respectively, to better than 0.2 pixels. Fig. 2 shows one of the roundabouts as recorded in the nadir-looking *Ikonos* image, along with a best-fitting ellipse to its edge points.

To complement the image mensuration via ellipse fitting, least-squares template matching was also employed within the stereo imagery, with special care being taken to alleviate problems such as target occlusions from shadowing and the presence of artifacts such as cars (e.g. Fig. 2). The matching utilised gradient images instead of grey values and observational weights were determined from the template gradients, i.e. only pixels along the circular template edge were used in matching, thus, making the method insensitive both to grey level variations within the roundabouts and to disturbances outside the roundabout perimeter. Three different template sizes were employed to accommodate the greatly varying roundabout sizes and in most cases an affine or conformal transformation was used. In spite of significant disturbances, and size and shape variations of roundabouts, the matching performed correctly in ca. 85% of the cases. Since the same template was matched simultaneously using the same parameters in all images, the image measurements were mutually quite consistent. This meant that parallax errors were reduced and height estimation accuracy could be expected to surpass that of the ellipse fitting method.

Table 1
Acquisition parameters for the 1-m *Ikonos Geo* panchromatic images of the Melbourne testfield

	Left stereo	Right stereo	Nadir
Date, time (local)	16/7/2000, 09:53	16/7/2000, 09:53	23/3/2000, 09:58
Sensor azimuth (°)	136.7	71.9	143.0
Sensor elevation (°)	61.4	60.7	83.4
Sun azimuth (°)	38.2	38.3	50.0
Sun elevation (°)	21.1	21.0	38.0

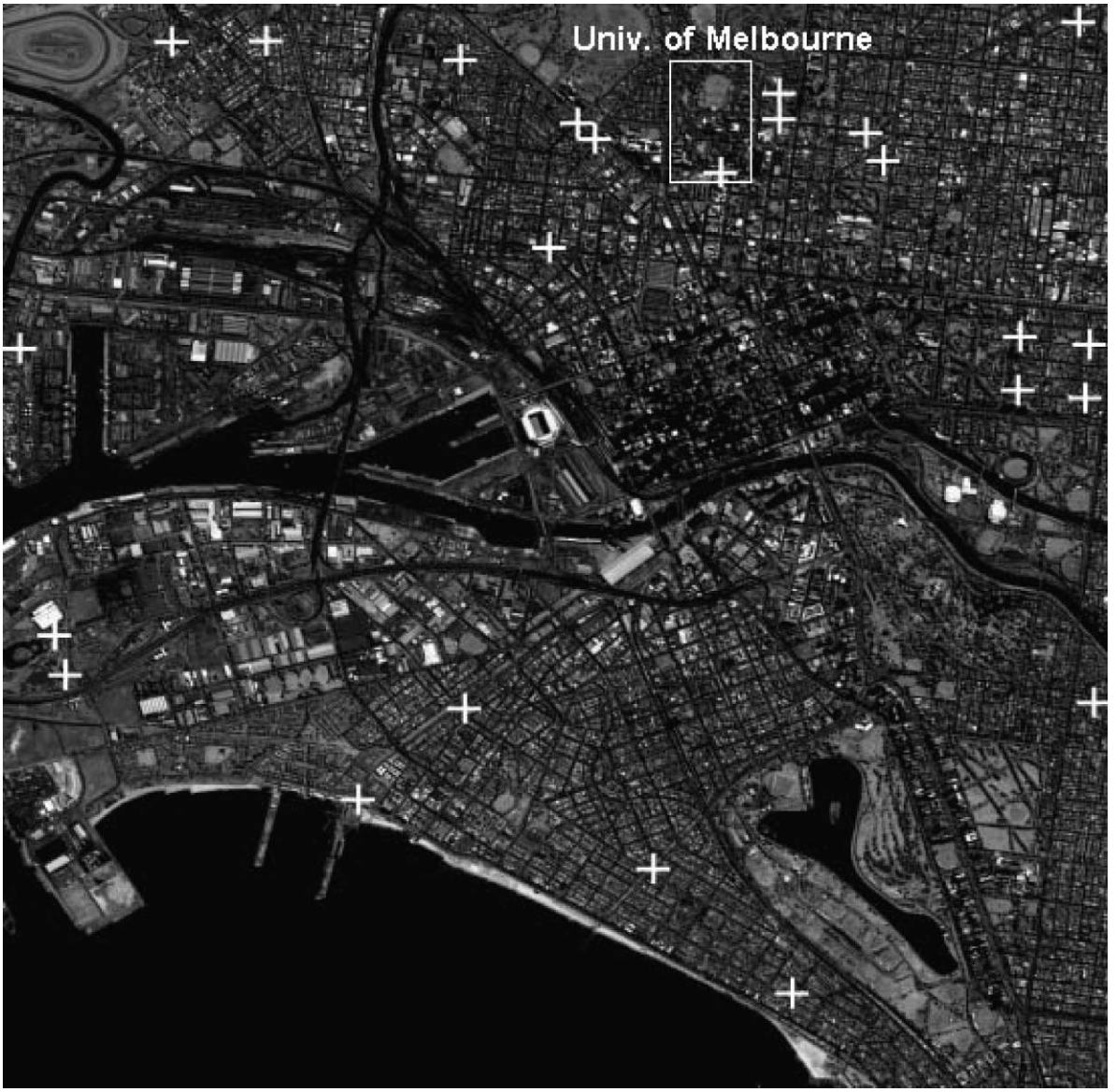

Fig. 1. *Ikonos Geo* panchromatic nadir image of Melbourne showing the distribution of control points and the University of Melbourne campus.

The images used for measurement were initially pre-processed for noise reduction and edge enhancement, as described in Section 3. An example of the modified least-squares matching is indicated in Fig. 3. The top row of the figure shows the template and the two stereo images with the starting (light) and final (dark) positions after a conformal transformation. The bottom row displays the matched gradients. This example illustrates the robustness of the process in the presence of both contrast variations and disturbances along the roundabout edge.

A second essential component of the Melbourne testfield in the context of city modelling comprised information on buildings. Due to both accessibility constraints and the unavailability of height data to submetre accuracy for central city high-rise buildings,

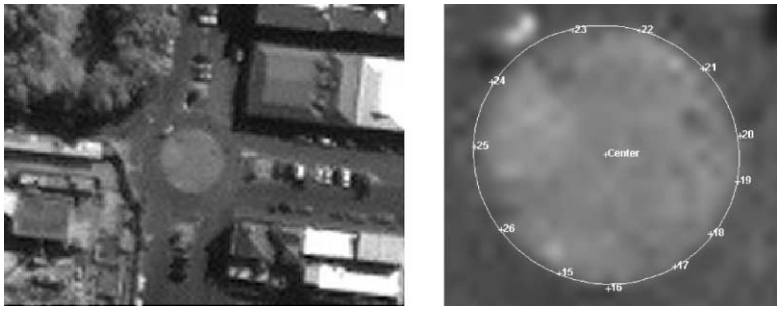

Fig. 2. *Ikonos* image of roundabout (left) and recorded edge points and best-fitting ellipse (right).

many over 30 stories, it was decided that the campus of the University of Melbourne would serve as the test site for the building reconstruction and visualisation phase of the project. The campus comprises a few dozen major buildings which vary in design characteristics, size, shape, roof superstructure and height, though most are between four and 10 stories tall. Building height data for 19 image-identifiable and readily accessible roof corners was provided to 10 cm accuracy through precise GPS surveys. This data formed the metric standard by which the 3D spatial intersection for building extraction would be assessed. Image coordinate observations to these feature points were carried out by manual recording, both in stereo and monoscopically (for the nadir image), nominally to 0.5–1 pixel precision. However, the definition of corner points was often weak, leading to the possibility of pixel-level errors. Least-squares matching was not appropriate for the recording of such corner features due to both occlusions and geometric differences between the images that could not be modelled through affine transformation.

An existing stereopair of 1:15,000 scale wide-angle colour aerial photography of the campus was employed

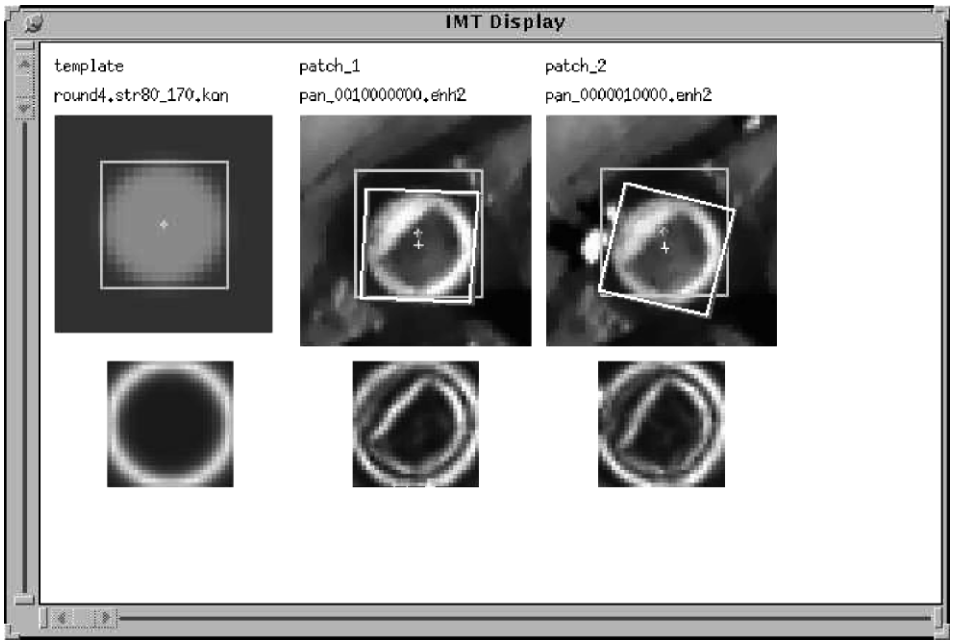

Fig. 3. An example of modified least squares template matching (see explanations in text).

in the evaluation of the building extraction potential of *Ikonos* imagery. This imagery had previously been used to create a reasonably detailed 3D model of the campus, which in regard to recoverable feature content could be compared to that derived from *Ikonos* data.

3. Radiometric aspects and image preprocessing

3.1. Radiometric quality analysis

Prior to discussing radiometric features of the *Ikonos* imagery, a subject which is discussed further in Baltsavias et al. (2001), it is noteworthy that operational aspects of the image acquisition are likely to have a more profound effect on the homogeneity or non-homogeneity of image quality than specific radiometric characteristics of the sensor system. For example, large changes in image quality and suitability for automated feature extraction are associated with variations in the sensor view angle, the sun angle and shadowing, the seasons, atmospheric conditions, and whether the scene is recorded in mono or stereo. These influences are well known, but it needs to be appreciated that with the exception of the last aspect, they are largely beyond the control of the image user. There is limited opportunity for the user to dictate specific imaging dates, times and weather conditions.

An example of the varying quality of two *Ikonos* images (from other projects) with similar sensor elevation but varying sun illumination and atmospheric conditions is shown in Fig. 4. Of the three Melbourne images employed, the near-nadir image was superior in terms of both contrast and visual resolution. This can be explained by the higher sensor and sun elevation, though it is uncertain if this fact alone accounted for the modest difference in image quality, or whether differences were in addition due to changes in atmospheric conditions or aspects of the epipolar resampling of the stereo images.

All images were preprocessed by Space Imaging with Modulation Transfer Function Compensation (MTFC) but no Dynamic Range Adjustment (DRA). Although the images were delivered as 11-bit data, the number of grey values having a substantial frequency was much less than 2048. For the left, right and nadir panchromatic images, grey values with a frequency of more than 0.01% covered only the ranges of 44–343, 56–423 and 61–589, respectively. The corresponding effective grey value ranges of 299, 367 and 528 (37, 46 and 66 grey values for a linear stretch to 8-bit) are quite similar to the effective intensity range observed

Fig. 4. *Ikonos Geo* panchromatic images of Lucerne, Switzerland (left), and Nisyros, Greece (right), exhibiting very different image quality and building definition.

with other spaceborne linear array CCD sensors such as SPOT and MOMS. The peak of the histogram is typically towards the darker region, with the right part of the histogram decreasing smoothly and slowly towards the higher intensity values.

The overall noise characteristics of the images (also noted with *Ikonos* images from other projects) were analysed in both homogeneous (sea surface) and nonhomogeneous areas (e.g. city) by a procedure explained in Baltsavias et al. (2001). The use of nonhomogeneous areas in image noise evaluation is justified as large homogeneous areas do not always exist. This process also allows an analysis of the noise variation as a function of intensity, as noise is not additive but multiplicative (i.e. intensity-dependent). The analysis revealed the presence of somewhat more noise than the four grey values reported by Space Imaging for raw panchromatic and multispectral images without MTFC (Gerlach, 2000) and the 3.5–5 grey values reported using on-board calibration and sun imaging (Cook et al., 2001), namely 1.5–10.5 grey values depending upon intensity and spectral type. The extent of the noise, however, was not judged to be of crucial significance for the specific task of building reconstruction. The noise level of the multispectral imagery was much lower than that of the panchromatic, with the pan-sharpened imagery being slightly more noisy than the panchromatic.

Geo images have been found to exhibit several artifacts in addition to their noise content, of which a number remain unexplained. Many are visible only in homogeneous areas, especially after contrast enhancement, and some appear in areas of rich texture. The artifacts often lead to small grey level variations (e.g. two to four grey values in 11-bit images), although after contrast enhancement to aid visual interpretation and measurement, or automated computer processing, they can lead to erroneous high-contrast texture patterns. Further details are provided in Baltsavias et al. (2001). The reported radiometric concerns are not related solely to the sensor imaging parameters but also to the subsequent image processing methods and to image compression. In order to optimize the downloading of an image, large homogeneous areas are compressed more, thus, leading to additional artifacts in such regions.

The MTFC used to reduce the image defocusing due to use of time delay and integration, especially in the scan direction (the direction in which the lines are collected), can cause ringing effects and so degrade edge detail. The compression to 2.6 bits also leads to some artifacts, which are more visible in homogeneous areas. Some additional problems include shadows and image saturation. The shadow areas in the Melbourne imagery did not have a significant signal variation and, thus, in spite of a strong contrast enhancement, feature details in shadow areas were often barely visible. Saturation occurred routinely, with bright vertical walls, especially those with surface normals approximately in the middle of the illumination-to-sensor angle. This led again to a loss of detail and poor definition and even to the disappearance of edges when two saturated walls were intersecting.

3.2. Image preprocessing

In order to reduce the effects of the above mentioned radiometric problems and optimise the images for subsequent computer processing to support the measurement of GCPs and buildings, various preprocessing methods were developed, implemented and tested. The full details of these are given in Baltsavias et al. (2001) and Figs. 5 and 6 illustrate the impact of the adopted image processing approaches. The first method consisted of an anisotropic Gaussian low-pass filtering to reduce noise and stripes in the scan direction (which for nonstereo images are almost vertical), coupled with application of a Wallis filter for contrast enhancement (Fig. 5, middle). The filter anisotropy was aimed at filtering more along the image lines in order to reduce vertical striping.

In a second preprocessing step, after the low-pass filtering, an unbiased anisotropic diffusion was used to further reduce noise and sharpen edges (Fig. 6). The improvement of the Wallis filter in shadow regions was not as much as previously achieved for aerial and other satellite imagery, possibly due to a low signal variation in these regions. Both these approaches were applied to 8-bit data that were generated by a linear compression of the original 11-bit imagery.

Later, a third, improved approach was adopted. Two adaptive local filters were first developed. They reduced noise, while sharpening edges and preserving even fine detail such as one-pixel wide lines, corners and end points of lines (compare edge sharpness in the lower two images of Fig. 6). Optionally, salt-and-

Fig. 5. Original image (left), after first preprocessing method (middle) and third preprocessing method (right).

pepper noise can be eliminated to a certain extent. The effect of the two local filters is generally quite similar, although they use a different size and number of masks, and one employs a fuzzy method. They require as input an estimate of the noise, which may be known or determined by the methods mentioned above. Using this approach, the noise was reduced to 30% of that exhibited by the original images. Next, a new version of the Wallis filter is applied and this estimates automatically some of the filter parameters. Finally, a reduction to 8-bit imagery by histogram equalisation is performed (Figs. 5 and 6), the histogram equalisation being iterative so as to occupy all eight bits with similar frequencies.

For the *Ikonos* imagery, processing in 11-bit led to slightly better 8-bit images than the first two preprocessing methods, even though the 11-bit data was effectively only 8–9 bits. The histogram equalisation, which is optimal for general computer processing but may lead to strong bright and dark regions for visual interpretation (see right image in Fig. 5), could be replaced through an optimisation of a selected target grey level range or by an alternative reduction of Gaussian type.

4. Metric quality

4.1. Accuracy potential

The recovery of 3D cartographic information from satellite line scanner imagery has been the subject of photogrammetric investigation for the last decade and a half. Mathematical models have been formulated to support bundle adjustment of cross-track *SPOT* and *IRS-1C/D* imagery, as well as *MOMS-02* three-line imagery which is an along-track configuration with similarities to the *Ikonos* coverage of the Melbourne testfield. Fully rigorous mathematical models for orientation and triangulation, which have in turn implied provision of sensor calibration data and, to a degree, prior information on the satellite orbit and sensor attitude data, have been a prerequisite for these developments. In summary, it could be said that under ideal conditions of high-quality image mensuration and ground control/checkpoints, coupled with favourable imaging geometry (e.g. $B/H > 0.8$) and provision of sensor calibration data, 3D point positioning accuracy corresponding to 0.3 of the pixel footprint is possible (Ebner et al., 1996) with medium-resolution stereo satellite imagery. However, accuracies of between 0.5 and 2 pixels are more commonly encountered in practical tests.

Through a simple extrapolation of these findings to 1-m resolution imagery, we might anticipate that under similar operational constraints submetre 3D positioning accuracy should be obtainable from stereo *Ikonos* panchromatic and pan-sharpened image data. Consider, for example, a stereo *Ikonos* configuration similar to that covering the Melbourne testfield. Under the assumption of an image measurement accuracy of 0.4 pixel ($\sigma_{XY} = 5$ μm), the optimal 3D point positioning precision to be anticipated for the stereo configuration is $\sigma_{XY} = 0.3$ m (planimetry) and $\sigma_Z = 0.7$ m (height). If this stereo geometry is extended to three along-track images (addition of a nadir-looking image), again as we have for the Melbourne testfield, the 3D positioning precision in Z remains unchanged (see also Ebner

Fig. 6. Top: original image (left) and after Wallis filtering to indicate noise content, especially in homogeneous areas (right). Bottom: preprocessing by the second (left) and third (right) methods.

et al., 1992), whereas the planimetric precision is improved to σ_{XY}= 0.25 m, or 1/4 of the ground sample distance.

4.2. Sensor orientation models

At the present time, however, the option of applying rigorous, collinearity-based image orientation and triangulation models to *Ikonos* data is effectively denied to the end-user of this imagery, since the necessary camera model (calibration data) and precise ephemeris data for the satellite are withheld as proprietary information. Alternative orientation/triangulation models are required, with the rational function model being currently supported (Grodecki, 2001; Grodecki and Dial, 2001; Yang, 2000; Hu and Tao, 2001). The 80 RPCs per image for the transformation from offset and scaled latitude, longitude and height to similarly normalised image line and sample coordinates are computed from a 3D object point grid and

the corresponding image coordinates. The object points are in turn derived via the rigorous sensor model and known exterior orientation, which may be refined by bundle adjustment (Grodecki and Dial, 2001). The RPCs can be expected to yield absolute accuracies in subsequent 3D point positioning that are consistent with the specifications for the particular class of *Ikonos* product, i.e. *Geo*, *Precision*, etc. RPCs for the *Geo* product, which are expected to produce an RMS positioning accuracy of about 25 m, are derived solely from satellite ephemeris and attitude data without the additional aid of ground control. As will be demonstrated, there is considerable scope for enhancing the absolute accuracy of *XYZ* data obtained via RPCs through post transformation of the object point coordinates to control points in order to remove exterior orientation biases. This transformation may in the simplest case be a coordinate translation, or it may comprise a 3D translation and rotation.

Other polynomial models, either simpler or more complicated than the RPCs, can be estimated with similar methods using a strict sensor model. Options include nonrational polynomials (e.g. Kratky, 1989; Baltsavias and Stallmann, 1992), interpolation techniques using known object-to-image transformations for regular object or image grids (OGC, 1999) or the Universal Image Geometry Model (OGC, 1999), which is an extension of the RPC model. However, Space Imaging is not currently offering such modelling options. Moreover, users cannot readily employ these alternative models since the *Ikonos* sensor model has not been released. A discussion of the use of rational functions for photogrammetric restitution is given in Dowman and Dolloff (2000). RPCs can be estimated by using GCPs and not through a reparameterisation of the rigorous sensor model, and this option is provided by some commercial photogrammetric systems. Other nonrational polynomial models (e.g. Kratky, 1989; Papapanagiotu and Hatzopoulos, 2000) can be similarly estimated. However, estimation of such polynomial coefficients using GCPs needs many control points that cover the entire planimetric and height range of the scene and this can be very difficult to achieve in practise, as well as being very costly. It can also lead to severe extrapolation errors and possible undulations between GCPs, especially with higher degree polynomials. As will be illustrated, the use of so-called terrain-dependent RPCs (Hu and Tao, 2001) is likely to be unwarranted for *Ikonos* imagery since alternative, straightforward models that yield high accuracy are available.

Beyond rational functions, there are further models displaying a favourable level of sensor independence, which can be employed in order to overcome the absolute accuracy limitations of RPCs. Potential approaches that take account to varying degrees of the mixed projective/parallel projection of linear CCD sensors include the direct linear transformation or DLT (El-Madanili and Novak, 1996; Savopol and Armenakis, 1998), an extended DLT form (Wang, 1999; Fraser et al., 2001, 2002), or the use of piece-wise DLT functions (Yang, 2001). A second option is affine projection (Okamoto et al., 1999; Fraser, 2000). The former is fundamentally a projective model, whereas the latter is better suited to *Ikonos*' nominally parallel along-scan projection. The very small field of view of the sensor of only 0.93° leads to the overall projection approaching skew parallel in CCD-line direction (in scan direction it is parallel), especially over smaller subscene areas. As it happens, both these models may be thought of as linear rational functions. In the case of the affine model, a perspective-to-affine transformation of the image may first be warranted in stereo scenes containing moderate to high relief variation, though this is more the case with sensors having a larger field of view than *Ikonos*, e.g. SPOT. The object-to-image transformation functions for the DLT and affine models are given, respectively, as:

$$x = (L_1X + L_2Y + L_3Z + L_4)/(L_9X + L_{10}Y + L_{11}Z + 1)$$

$$y = (L_5X + L_6Y + L_7Z + L_8)/(L_9X + L_{10}Y + L_{11}Z + 1) \quad (1)$$

and

$$x = A_1X + A_2Y + A_3Z + A_4$$

$$y = A_5X + A_6Y + A_7Z + A_8 \quad (2)$$

where x and y are image space coordinates in the scan and line-CCD direction, respectively, and X, Y and Z are Cartesian object space coordinates. For both the two-

and three-image orientation/triangulation computations with the DLT and affine models, all parameters can be determined simultaneously. Further details are provided in Fraser et al. (2001). Additional parameters can be included in the model of Eq. (1) to account for nonlinearities in the DLT formulation for line scanner imagery. In the present investigation, however, it was found that such an extended form, as suggested by Wang (1999), did not yield any measurable accuracy improvement over the standard DLT model.

A variant to the 3D affine model, here called relief-corrected affine transformation, is similar but not identical to the affine projection of Eq. (2). It explicitly takes into account that *Geo* imagery is rectified to an inflated ellipsoid and map projected without terrain relief corrections. To relate object information to such imagery, the object coordinates can first be corrected by relief displacements using a flat or curved Earth model. A simple affine transformation can then relate object and image space without the need to apply any image transformation (from central perspective to affine to account for terrain relief). In fact, since the relative accuracy of *Geo* images is at the submetre level, as will be shown here, the major correction needed is a shift between the two spaces. The two scale and shear terms are required to model smaller deviations between the two spaces. It was found in tests involving various *Geo* images that in affine transformation between the two spaces, with GCPs in different projection systems, the two scale terms deviated from unity in the fourth or fifth decimal place only. Also, the rotation was of the order of $1-2^\circ$ (except of course for stereo images which are rotated) and nonorthogonality of the axes ranged from 0.003 to 0.03°. The projection of the GCPs onto a reference plane leads to corrections of the planimetric X and Y coordinates according to Eq. (3):

$$\Delta X = -(Z - Z_o)\sin a/\tan e$$
$$\Delta Y = -(Z - Z_o)\cos a/\tan e \quad (3)$$

where Z is the height of a given ground point, Z_o the height of the reference plane, a the sensor azimuth, e the sensor elevation and ΔX and ΔY the planimetric displacements of the object point due to projection onto the reference plane. The azimuth and elevation values can be obtained from the metadata file delivered with the *Geo* images.

The choice of the reference height plane can be arbitrary and the distribution of the GCPs is not critical so long as the affine parameters can be determined reliably. This can be achieved if the range of their coordinates in two nominally orthogonal directions covers approximately a third or more of the area imaged. In the reported implementation, the projection to the reference plane and the affine transformation are combined in a single operation involving eight parameters, just as in Eq. (2), though only six coefficients are independent since

$$A_3 = -(A_1 \sin a + A_2 \cos a)/\tan e$$
$$A_7 = -(A_5 \sin a + A_6 \cos a)/\tan e \quad (4)$$

The relief-corrected affine transformation can be used not only for object-to-image transformation and orthoimage generation (Kersten et al., 2000; Baltsavias et al., 2001), but also for 3D spatial intersection and automatic DSM generation using two or more images, including application to constrained image matching and epipolar resampling. The effective reduction in the number of parameters from the eight of Eq. (2) to the six of Eq. (4) is possible because the sensor elevation and azimuth are known. Thus, advantages of the approach are the need for fewer GCPs and the limited influence of their distribution. In addition, if GCPs along a water body are selected, the height need be known for only one GCP.

For the DLT and two affine models, the parameters (including sensor azimuth and elevation that vary very little within a scene) are considered constant for the full scene. This is appropriate for the normal scanning mode of *Ikonos* and for the three images evaluated, which were all north-to-south scans. The normal forward scanning mode of *Ikonos* is in N–S strips, termed containers by SI, where the sensor elevation and azimuth, although given for every scene of the strip, are constant within each strip. Multiple neighbouring strips can be acquired during one pass, each strip having different azimuth and possibly elevation. This N–S scan is typical for *Ikonos* images and should not be confused with the flight or track direction which differ. *Ikonos* can also scan in the reverse mode, i.e. from S to N, by continuously varying the elevation (but with constant azimuth). Although the satellite is agile,

it is unknown to the authors whether *Ikonos* can image one scene while also varying the azimuth.

The scanning in directions other than N–S or S–N, e.g. in W–E, would require a change of both elevation and azimuth. Examination of many images in the Carterra Online Catalogue of SI USA, including emergency cases like the Manhattan images of 12 September 2001 and southeastern Hainan images of April 2001 has, however, shown that *Ikonos* images are even in these cases in a N–S direction. When an area (strip) needs to be covered in directions other than N–S or W–E, this can be achieved by rotating the satellite and the sensor with respect to the N–S direction (effectively applying a kappa rotation), see, e.g. Manhattan images of 12 September 2001. Thus, any area can be imaged while still keeping azimuth and elevation constant within each strip. Even if imaging with continuous change of elevation and azimuth would be possible, it does not necessarily lead to coverage of a larger area, requires power consumption for the satellite manouvering, can lead to image quality deterioration though oversampling or undersampling if imaging and satellite manouvering are not perfectly synchronised, and leads to varying elevation and, thus, also to different image quality within a scene. It is also interesting to note that based on SI investigations (Cook et al., 2001), the reverse scan mode showed much poorer planimetric accuracy than the forward mode for Level 4a standard orthorectified products (without use of GCPs).

Based on the Carterra Online data, our assumption of constant elevation and azimuth seems to be fulfilled for each strip. Furthermore, even if this were not the case, we could still process long strips with our linear models, as long as for each scene (typically 11 by 11 km) elevation and azimuth are constant. This would require use of a different set of model parameters for each scene. If, however, we keep one set of model parameters for all scenes of a strip, the DLT and affine models, being linear approximations to higher-order rational functions, can be expected to show limitations, especially as the area covered by the *Ikonos* strip becomes long and, thus, the constant angle model may need extension via time-dependent parameters (e.g. Okamoto et al., 1999). Similarly, if elevation and azimuth vary within one scene, accurate orientation may require higher-order models. As will be illustrated, however, in the 50-km^2 Melbourne testfield all three models yielded submetre 3D positioning accuracy when applied with as few as three to six GCPs.

4.3. Planimetric positioning

In many respects, a prerequisite to the application of approaches such as affine projection and the DLT is that the imagery itself is of high metric integrity. As a means of both ascertaining the planimetric positioning accuracy of 1-m *Ikonos* imagery and of evaluating 'sensor linearity,' a number of 2D transformations (similarity, affine and projective) from image to object space were performed. The aim was to examine the accuracy in *XY* coordinates resulting from mapping the image data to height-corrected planes using various GCP configurations. The results of this 2D accuracy analysis, which are reported in more detail in Hanley and Fraser (2001), were very encouraging. For three configurations of six GCPs and 20–25 independent checkpoints, RMS positioning accuracies of 0.3–0.5 m were obtained. When a best-fit mapping was carried out using all 32 GCPs, the *XY* discrepancies displayed RMS values ranging from 0.27 to 0.38 m, i.e. from about 0.3 to 0.4 pixels.

Furthermore, the GCPs without projection to a plane were transformed with RPCs to image space and compared to the measured image coordinates (Baltsavias et al., 2001). While the absolute errors had a high bias of 29 and 16 pixels for the x and y pixel coordinates, respectively, the standard deviations were 0.4–0.6 pixels, showing a high relative accuracy for the RPCs. Although the 2D affine model with height-corrected GCPS is effectively equivalent to the explicit relief-corrected affine transformation, the latter was applied with a reference height of sea-level and transformations beyond 2D affine, namely bilinear, quadratic and biquadratic were employed using all available GCPs. The *XY* accuracy results were practically identical for all transformations being 0.41/0.46/0.36 and 0.60/0.60/0.45 pixels, respectively, for the ellipse fit and matching datasets for the left/right/nadir images.

The nadir image gave better results probably due to the better image quality and more accurate relief correction, since height errors influence the relief displacement by some five times less than in the stereo images due to the higher sensor elevation. One feature of note with the relief-corrected affine model was that

a configuration of three GCPS gave similar accuracies to six or eight control points. This provided a confirmation that the most important factor is GCP quality rather than quantity. The results with three GCPs, which had good but not optimal distribution, were worse than the 32-point GCP case by only 14% and 24% for the stereo and nadir images, respectively. This illustrated that three highly accurate GCPs with a reasonable distribution can yield subpixel accuracy in the transformation from object to image space.

In the absence of any camera model information, it was felt that the reported 2D analysis gave a strong indication of the metric integrity of *Ikonos Geo* imagery, which augured well for the use of linear and DLT models in 3D point positioning. Moreover, the tests demonstrated that in the presence of good quality control and DTM data (or moderately flat terrain) a single *Ikonos* image can readily yield an *XY* positioning accuracy of 0.5 pixel or better, whether it be for point positioning or ortho-image generation (e.g. Baltsavias et al., 2001).

4.4. 3D positioning of roundabouts

4.4.1. Rational functions

As a first step in analysing the 3D spatial intersection accuracy of *Ikonos* stereo images, 3D coordinates for the GPS-surveyed roundabouts were computed using the supplied RPCs, for the cases of both manually measured image coordinates (via ellipse fitting) and least-squares template matching. The 3D spatial intersection is computed by least-squares adjustment with initial approximations derived using just the linear terms of the RPCs (see details in Baltsavias et al., 2001; Fraser et al., 2002). The resulting RMS discrepancy in *XYZ* ground point coordinates averaged 8, 32 and 2 m in *X*, *Y* and *Z*, respectively, which was largely consistent with *Geo* specifications. The presence of a positioning bias close to the RMS values was clearly apparent, however, and a simple coordinate translation using six control points reduced the RMS discrepancy at remaining checkpoints to 0.4–0.6 m in planimetry and 0.6–0.8 m in height. A 2D translation (bias removal) in image space using six GCPs and subsequent 3D spatial intersection using the RPCs gave similar results to the translation in object space. As shown in Fraser et al. (2002), it is also possible to recover image coordinate biases via an additional parameter approach, which is particularly well suited to multiimage configurations where the bias characteristics for each image are different.

The results obtained compare very favourably to the 1–2-m planimetric and height accuracy reported for *Ikonos Precision* imagery in Grodecki and Dial (2001) and surpass those from investigations employing *Geo* imagery that have utilised more, but less precise, ground control points and RPCs (Hu and Tao, 2001) or proprietary sensor models (Toutin et al., 2001). In regard to a comparison of results obtained from least-squares matching and ellipse fitting, the image coordinates obtained from matching were slightly worse due to some unmodelled disturbances of the roundabout perimeters, but they yielded more consistent accuracy in height determination.

Computations of 3D spatial intersection for the 32 roundabouts within the Melbourne *Ikonos* testfield, which are further discussed in Baltsavias et al. (2001) and Fraser et al. (2001), confirmed that high relative accuracies are attainable with *Geo* RPCs in spite of their rather modest absolute accuracy specification. Provision of only one or two GCPs facilitated removal of positioning biases, which were much larger in planimetry than height, to yield 1–2-m level 3D positioning accuracy, whereas subpixel accuracies were achieved with additional GCPs. The results were insensitive in the selection of the GCPs used to remove the bias, as long as they were fairly well distributed. It should be noted though that RPCs have until recently been provided by Space Imaging as a standard product for stereo imagery only. Since July 2001, RPCs have been made available with the *Geo* OrthoKit product, but this is considerably more expensive than the standard *Geo* product (OrthoKit is currently offered by Space Imaging at a 61–85% surcharge).

4.4.2. Affine projection and DLT models

With the affine projection and DLT orientation/triangulation models it is a straightforward matter to extend the analysis of stereo *Ikonos* imagery to an evaluation of three-image configurations. A series of bundle[1] adjustments were computed using both the DLT (Eq. (1)) and the affine projection model (Eq.

[1] Strictly speaking, the term bundle should be used for a two-dimensional sensor only, but here we use it also for linear CCDs.

(2)). A full account of the results is beyond the scope of the present paper and readers are referred to Fraser et al. (2001, 2002) for further details. The results can, however, be summarised as follows: For control configurations of four, six and eight GCPs and 20–25 checkpoints, the affine model produced RMS 3D positioning accuracies of 0.3–0.5 m in *XY* and 0.5–0.7 m in *Z*, for both stereo and three-image geometries. Accuracy deteriorated only slightly with decreasing numbers of control points, while use of three instead of two images improved the results, especially in height. For the same number of control points, the affine model yielded slightly better results than the RPC-based spatial intersection. For the same GCP sets, the DLT yielded slightly lower 3D positioning accuracy of 0.3–0.6 m in *XY* and 0.5–0.9 m in *Z*, and it was found to exhibit stability problems for certain GCP configurations. The fact that first-order models can readily yield subpixel positioning accuracy is very encouraging for both metre-level city modelling applications and for GIS mapping for local government planning and management, which requires nominal 1σ precision of 1.5–2 m (e.g. Davis and Wang, 2001).

4.4.3. Relief-corrected affine transformation

We consider the relief-corrected affine model separately since this method did not employ simultaneous computation of transformation parameters and object point coordinates. Instead, a two-stage 3D spatial resection/intersection approach was followed. The affine transformations that were computed for each image independently (Section 4.2) utilised six parameters as the parameters A_3 and A_7 were computed by Eq. (4). The final eight affine parameters (Eq. (2)) were then used with the same algorithm for 3D spatial intersection that was employed for the RPCs (see Section 4.4.1), though without bias removal. The RMS errors in planimetry and height, using the ellipse fit dataset and two images were 0.43 and 0.76 m for three GCPs, and 0.45 and 0.71 m for eight GCPs. This illustrates the small influence of the number of GCPs upon achievable accuracy. The results using all three images were better, being 0.32 and 0.57 m, and 0.33 and 0.60 m for 3- and 8-point GCP configurations, respectively.

In all cases, planimetric accuracy was in the 0.3–0.5-m range and height accuracy in the 0.6–0.8-m range. The results are very similar to those of the 'standard' affine projection, however, some differences exist. Affine projection (Eq. (2)) estimates eight parameters using the measured *XYZ* coordinates of GCPs along with bundle adjustment, whereas the relief-corrected approach involves only six independent parameters for each image and it employs corrected planimetric coordinates of GCPs (Eq. (3)). The latter approach needs only three GCPs and requires no image pretransformation from central perspective to affine projection. The use of bundle adjustment for determining the six relief-corrected affine parameters could be favourably used but it has not as yet been implemented.

5. Building extraction

Whereas the foregoing 3D point positioning evaluation was centred upon high-quality targets, accurate positioning of building features, generally corners and edges, involves not only metric factors but issues of image resolution and feature identification. The approach adopted in this investigation for ascertaining the metric quality of building extraction in stereo *Ikonos* imagery again involved independent checks of photogrammetrically triangulated, distinct points against their GPS-surveyed positions. As mentioned, 19 image-identifiable roof corners were precisely surveyed to serve as accuracy checkpoints in the building extraction phase.

Within the stereo spatial intersection of roof corners, the RPCs produced RMS accuracies of 0.7 m in planimetry and 0.9 m in height after removal of the bias in object space using six GCPs. Corresponding accuracy estimates resulting from the 19 checkpoints for the affine projection and DLT models with six GCPs were 0.6 and 0.7 m in planimetry, and 0.8 and 1.0 m in height, respectively. Spatial intersection of the threefold image coverage produced results that were not significantly different than those for the stereo restitution. Whereas in practice it is unlikely that a three-image coverage would be employed for building extraction, provision of the near-nadir image can prove very useful for subsequent ortho-image generation over built-up urban areas.

In order to provide a qualitative and more extensive quantitative assessment of the potential of stereo

Ikonos imagery for the generation of building models, the University of Melbourne campus was measured manually in stereo using an in-house developed software tool for the *Ikonos* stereo images, and an analytical plotter for the 1:15,000 colour aerial imagery. The resulting plots of extracted building features are shown in Fig. 7. The manual measurements of roof corners and points of detail were topologically structured automatically using the software package CC-Modeler (Gruen and Wang, 1998) and also visualised as indicated by Fig. 8.

A comparison of the two models in Fig. 7, one from aerial photography and the other from *Ikonos* 1-m imagery, reveals the following regarding the *Ikonos* stereo feature extraction: About 15% of the buildings measured in the aerial images could not be modelled and it is interesting to note that this figure fits well to the findings of Ridley et al. (1997). Also, a number of both small and large buildings could not be identified and measured, though some new buildings could, however, be reconstructed, even if small. Finally, as indicated in Fig. 9, buildings could often only be generalised with a simplified roof structure and variations to their form and size. Measurement and interpretation in stereo proved to be a considerable advantage, and we expect that colour imagery would also have been very advantageous were it available. Other factors influencing the feature extraction process are shadows, occlusions,

Fig. 7. Buildings of University of Melbourne campus reconstructed from 1:15,000 aerial images (left) and stereo *Ikonos* imagery (right). To simplify visualisation, first points and first lines have been omitted in the left figure.

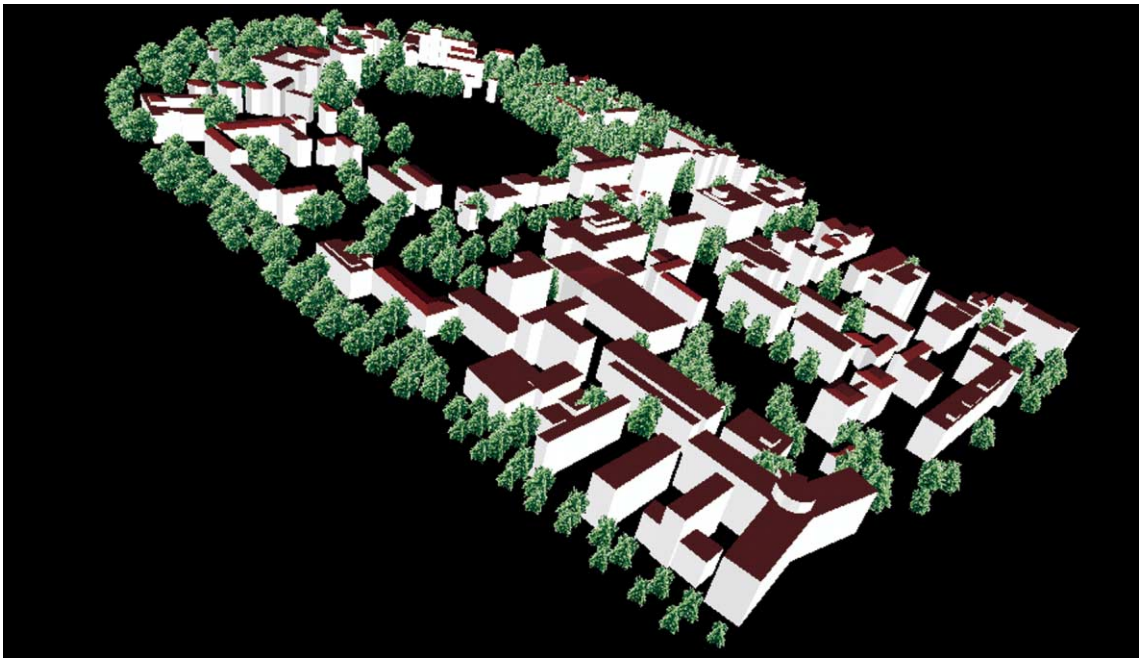

Fig. 8. Visualisation from stereo *Ikonos* images of extracted buildings and trees of University of Melbourne campus.

edge definition (related also to noise and artifacts), saturation of bright surfaces, sun and sensor elevation and azimuth, and atmospheric conditions. The 1-m resolution of *Ikonos* also leads to certain interpretation restrictions. This investigation was aimed in part at quantifying the extent of such limitations. However, additional tests with different *Ikonos* stereo imagery are needed in order to draw more comprehensive conclusions.

6. Conclusions

The reported investigation has shown that *Geo* stereo and three-image configurations have the potential to yield submetre accuracy in both planimetry and height without a requirement for provision of the *Ikonos* camera model and orbit ephemeris data. Moreover, this high level of accuracy is obtained with straightforward linear and DLT orientation models at

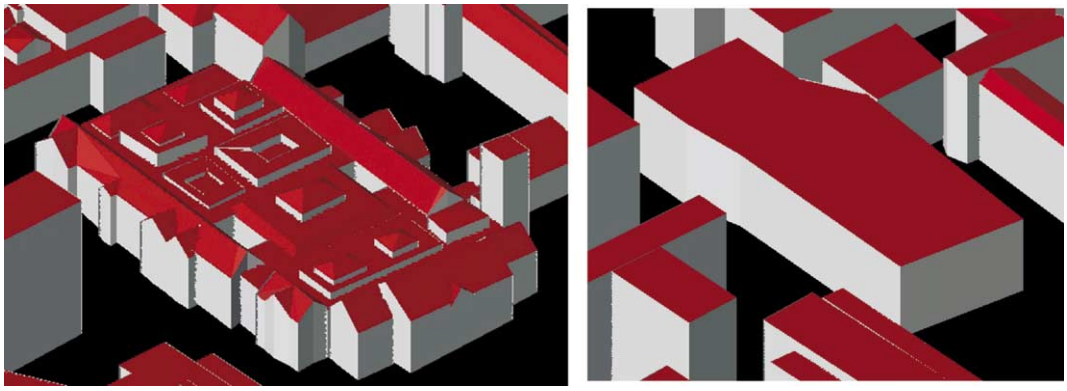

Fig. 9. Building with complicated roof structure as extracted from stereo aerial (left) and *Ikonos* images (right).

the modest cost of providing a small number of, say, three to six GCPs with dm accuracy. As regards alternative sensor orientation models, it has been shown that RPCs with bias removal, affine projection, the DLT and relief-corrected affine transformation are all suited to high-accuracy 3D positioning, with accuracy for two and three images reaching 0.3–0.6 m in planimetry and 0.5–0.9 m in height. In fact, the two affine model approaches yielded the most accurate results within the 7×7-km Melbourne testfield, showing that the *Geo* product (without RPCs) can be used for 3D point positioning and object extraction to a precision normally associated with only the most expensive *Ikonos* product, *Precision Plus* imagery.

The results obtained are encouraging but must be weighed against some notable shortcomings of 1-m satellite imagery, especially for the reported case of building feature detection and identification. While the limitations of an image resolution of 1 m are well understood, it is more the variability of image quality from scene to scene that will limit application to building reconstruction and city modelling. The influence of factors which are largely beyond the current control of the image user, such as date and time of image collection, specification of favourable sun angles and atmospheric conditions, etc. will likely generate difficulties if one is seeking to exploit the imagery to its full potential. Problems were encountered in this investigation, not only in identifying all buildings of a certain size, but also in accurately reconstructing their form without excessive generalisation. The shortcomings in radiometric quality, although not of major concern in the present study, also give rise to accuracy and interpretability concerns in both manual and computer mensuration. However, the issues of radiometric inhomogeneity, both within and between *Ikonos* scenes, are unlikely to be affected by the level of image product purchased and this investigation has demonstrated that very high metric performance is achievable with the least expensive product offering, namely *Geo* imagery.

Acknowledgements

The computational and general research support of Harry Hanley and Takeshi Yamakawa at the University of Melbourne, and Maria Pateraki and Li Zhang at ETH Zurich, in this collaborative project is gratefully acknowledged. The *Ikonos* image of Lucerne was kindly provided by the National Point of Contact, Swiss Federal Office of Topography, while the *Ikonos* image of Nisyros was made available by Prof. E. Lagios, University of Athens, Greece, within the EU project Geowarn.

References

Baltsavias, E., Stallmann, D., 1992. Metric information extraction from SPOT images and the role of polynomial mapping functions. Int. Arch. Photogramm. Remote Sens. 29 (B4), 358–364.

Baltsavias, E., Pateraki, M., Zhang, L., 2001. Radiometric and geometric evaluation of Ikonos GEO images and their use for 3D building modelling. Proc. Joint ISPRS Workshop "High Resolution Mapping from Space 2001," Hannover, 19–21 September. Institute of Photogrammetry & Geoinformation, University of Hannover, 21 pp. (on CD ROM).

Cook, M.K., Peterson, B.A., Dial, G., Gerlach, F., Hutchins, K., Kudola, R., Bowen, H., 2001. IKONOS technical performance assessment. Proc. SPIE 4381, 94–108.

Davis, C.H., Wang, W., 2001. Planimetric accuracy of Ikonos 1-m panchromatic image products. Proc. ASPRS Annual Conference, St. Louis, 23–27 April. American Society of Photogrammetry & Remote Sensing, 14 pp. (on CD ROM).

Dial, G., 2000. Ikonos satellite mapping accuracy. Proc. ASPRS Annual Conference, Washington, DC, 22–26 May. American Society of Photogrammetry & Remote Sensing, 8 pp. (on CD ROM).

Dial, G., Gibson, L., Poulsen, R., 2001. IKONOS satellite imagery and its use in automated road extraction. In: Baltsavias, E., Gruen, A., Van Gool, L. (Eds.), Automated Extraction of Man-Made Objects from Aerial and Space Images (III). Balkema Publishers, Lisse, pp. 357–367.

Dowman, I., Dolloff, J.T., 2000. An evaluation of rational functions for photogrammetric restitution. Int. Arch. Photogramm. Remote Sens. 33 (B3/1), 252–266.

Ebner, H., Kornus, W., Ohlhof, T., 1992. A simulation study on point determination for the MOMS-02/D2 space project using an extended functional model. Int. Arch. Photogramm. Remote Sens. 29 (B4), 458–464.

Ebner, H., Ohlhof, T., Putz, E., 1996. Orientation of MOMS-02/D2 and MOMS-2P imagery. Int. Arch. Photogramm. Remote Sens. 31 (B3), 158–164.

El-Madanili, Y., Novak, K., 1996. Precise rectification of SPOT imagery using the direct linear transformation model. Photogramm. Eng. Remote Sens. 62 (1), 67–72.

Fraser, C.S., 2000. High-resolution satellite imagery: a review of metric aspects. Int. Arch. Photogramm. Remote Sens. 33 (B7/1), 452–459.

Fraser, C.S., Hanley, H.B., Yamakawa, T., 2001. Sub-metre geopositioning with Ikonos GEO imagery. Proc. Joint ISPRS Workshop "High Resolution Mapping from Space 2001," Hannover,

19–21 September. Institute of Photogrammetry & Geoinformation, University of Hannover, 8 pp. (on CD ROM).

Fraser, C.S., Hanley, H.B., Yamakawa, T., 2002. 3D positioning accuracy of Ikonos imagery. Photogramm. Rec. 17 (99) (in press).

Gerlach, F., 2000. Characteristics of space imaging's one-meter resolution satellite imagery products. Int. Arch. Photogramm. Remote Sens. 33 (B1), 128–135.

Grodecki, J., 2001. Ikonos stereo feature extraction—RPC approach. Proc. ASPRS Annual Conference, St. Louis, 23–27 April. American Society of Photogrammetry & Remote Sensing, 7 pp. (on CD ROM).

Grodecki, J., Dial, G., 2001. Ikonos geometric accuracy. Proc. Joint ISPRS Workshop "High Resolution Mapping from Space 2001," Hannover, 19–21 September. Institute of Photogrammetry & Geoinformation, University of Hannover, 10 pp. (on CD ROM).

Gruen, A., 2000. Potential and limitations of high-resolution satellite imagery. Keynote Address, 21st Asian Conference on Remote Sensing, Taipei, 4–8 December, 13 pp.

Gruen, A., Wang, X., 1998. CC-Modeler: a topology generator for 3-D city models. ISPRS J. Photogramm. Remote Sens. 53 (5), 286–295.

Hanley, H.B., Fraser, C.S., 2001. Geopositioning accuracy of Ikonos imagery: indications from 2D transformations. Photogramm. Rec. 17 (98), 317–329.

Hofmann, P., 2001. Detecting buildings and roads from IKONOS data using additional elevation information. GIS (6), 28–33.

Hu, Y., Tao, V., 2001. 3-D reconstruction algorithms with the rational function model and their applications for Ikonos stereo imagery. Proc. Joint ISPRS Workshop "High Resolution Mapping from Space 2001," Hannover, 19–21 September. Institute of Photogrammetry & Geoinformation, University of Hannover, 12 pp. (on CD ROM).

Jacobsen, K., 2001. Automatic matching and generation of orthophotos from airborne and spaceborne line scanner images. Proc. Joint ISPRS Workshop "High Resolution Mapping from Space 2001," Hannover, 19–21 September. Institute of Photogrammetry & Geoinformation, University of Hannover, 9 pp. (on CD ROM).

Kersten, T., Baltsavias, E., Schwarz, M., Leiss, I., 2000. Ikonos-2 Carterra Geo-Erste geometrische Genauigkeitsuntersuchungen in der Schweiz mit hochaufgeloesten Satellitendaten. Vermessung, Photogrammetrie, Kulturtechnik (8), 490–497.

Kratky, V., 1989. On-line aspects of stereophotogrammetric processing of SPOT images. Photogramm. Eng. Remote Sens. 55 (3), 311–316.

Muller, J.P., Kim, J.R., Tong, L., 2001. Automated mapping of surface roughness and landuse from simulated and spaceborne 1 m data. In: Baltsavias, E., Gruen, A., Van Gool, L. (Eds.), Automated Extraction of Man-Made Objects from Aerial and Space Images (III). Balkema Publishers, Lisse, pp. 369–379.

OGC, 1999. The Open GIS™ abstract specification. Vol. 7: The Earth imagery case. Available at http://www.opengis.org/public/abstract/99-107.pdf (accessed 1 November, 2001).

Okamoto, A., Ono, T., Akamatsu, S., Fraser, C.S., Hattori, S., Hasegawa, H., 1999. Geometric characteristics of alternative triangulation models for satellite imagery. Proc. ASPRS Annual Conference, Portland, Oregon, 17–21 May. American Society of Photogrammetry & Remote Sensing, 12 pp. (on CD ROM).

Papapanagiotu, E.G., Hatzopoulos, J.N., 2000. Automatic extraction of 3D model coordinates using digital stereo images. Int. Arch. Photogramm. Remote Sens. 33 (B4/2), 805–812.

Ridley, H.M., Atkinson, P.M., Aplin, P., Muller, J.P., Dowman, I., 1997. Evaluating the potential of the forthcoming commercial US high-resolution satellite sensor imagery at the Ordinance Survey. Photogramm. Eng. Remote Sens. 63 (8), 997–1005.

Savopol, F., Armenakis, C., 1998. Modelling of the IRS-1C satellite pan imagery using the DLT approach. Int. Arch. Photogramm. Remote Sens. 32 (4), 511–514.

Sohn, G., Dowman, I., 2001. Extraction of buildings from high resolution satellite data. In: Baltsavias, E., Gruen, A., Van Gool, L. (Eds.), Automated Extraction of Man-Made Objects from Aerial and Space Images (III). Balkema Publishers, Lisse, pp. 345–355.

Toutin, T., 2001. Geometric processing of Ikonos Geo images with DEM. Proc. Joint ISPRS Workshop "High Resolution Mapping from Space 2001," Hannover, 19–21 September. Institute of Photogrammetry & Geoinformation, University of Hannover, 9 pp. (on CD ROM).

Toutin, Th., Cheng, P., 2000. Demystification of IKONOS! EOM 9 (7), 17–21.

Toutin, Th., Chénier, R., Carbonneau, Y., 2001. 3D geometric modelling of Ikonos GEO images. Proc. Joint ISPRS Workshop "High Resolution Mapping from Space 2001," Hannover, 19–21 September. Institute of Photogrammetry & Geoinformation, University of Hannover, 9 pp. (on CD ROM).

Wang, Y., 1999. Automated triangulation of linear scanner imagery. Proc. Joint ISPRS Workshop "Sensors and Mapping from Space," Hannover, 27–30 September. Institute of Photogrammetry & Geoinformation, University of Hannover, 5 pp. (on CD ROM).

Yang, X., 2000. Accuracy of rational function approximation in photogrammetry. Proc. ASPRS Annual Conference, Washington D.C., 22–26 May. American Society of Photogrammetry & Remote Sensing, 10 pp. (on CD ROM).

Yang, Y., 2001. Piece-wise linear rational function approximation in digital photogrammetry. Proc. ASPRS Annual Conference, St. Louis, 23–27 April. American Society of Photogrammetry & Remote Sensing, 14 pp. (on CD ROM).